mater.scichina.com link.springer.com

Published online 7 April 2022 | https://doi.org/10.1007/s40843-021-1984-8
Sci China Mater 2022, 65(9): 2393–2400

Regeneration of spent cathodes of Li-ion batteries into multifunctional electrodes for overall water splitting and rechargeable Zn-air batteries by ultrafast carbothermal shock

Xuerong Zheng[1,2,3], Xin Zhao[2], Junda Lu[1], Jihong Li[1], Zhengpei Miao[1], Wei Xu[4], Yida Deng[1,3*] and Andrey L. Rogach[2]

ABSTRACT Lithium-ion batteries (LIBs) are widely used in electric vehicles and consumer electronics and require reliable recycling strategies. In this paper, we investigated how an ultrafast carbothermal shock treatment can be used to convert spent cathodes of LIBs ($LiNi_{0.8}Mn_{0.1}Co_{0.1}O_2$) into Ni/Ni-Mn-Co-O (N/NMCO) composites with a remarkable electrocatalytic performance toward oxygen evolution, oxygen reduction, and hydrogen evolution reactions. The converted spent cathodes can be employed as cathodes and anodes in an overall water-splitting system, and they displayed a low overpotential of 1.61 V and remarkable stability at different current densities. Moreover, N/NMCO electrodes can be used as cathodes in rechargeable Zn-air batteries, which displayed long-term stability (>30 h), high specific capacity (781 mA h g^{-1}) and peak power density (137 mW cm^{-2}), as well as a small charge/discharge voltage gap of 0.71 V. Thus, our study offers a "waste-to-treasure" strategy for the regeneration of spent cathodes of LIBs and their applications in other advanced energy storage and conversion technologies.

Keywords: lithium-ion battery, waste management, carbothermal shock, overall water splitting, Zn-air battery

INTRODUCTION

The Paris Agreement (2015) on climate change offered the course for the world to transfer to low-carbon technologies, as major economies declared the deadlines for reducing CO_2 emission and achieving carbon neutrality. To achieve these goals, accelerated efforts are desired to advance clean-energy conversion techniques, such as photovoltaic cells and wind-driven generators, and energy storage systems. Lithium-ion batteries (LIBs) became a pervasive energy storage system that enabled electricity utilization due to their long-cycling stability, high power density, and energy efficiency. The application areas of LIBs cover consumer electronics, electric vehicles and grids, which results in a fast-increasing demand on such batteries, with an average growth rate of over 39% annually, and their global shipment volume is expected to reach 440 GW h in 2025 [1,2]. Thus, sustainability concerns related to the recycling and regeneration of LIBs are receiving increasing attention. Given that the lifetimes of LIBs last for about 2–3 years for consumer electronics and 5–8 years for electric vehicles [1–3], large numbers of spent batteries are expected to be regenerated; such waste is hazardous because of the high content of heavy metals and organic electrolytes. On the other hand, spent batteries also contain significant amounts of valuable metals, such as Li, Ni, Co, and Mn, which should be recycled and reused to alleviate the depletion of strategic metal resources [4,5]. Therefore, a closed-loop LIB recycling technology must be exploited to minimize the potential environmental pollution and improve the reutilization of valuable metals, in particular from the spent cathodes containing most of the recyclable elements in LIBs.

The common waste-management strategies include disposal, recovery, reuse, and recycling; the last two strategies are applicable for spent LIB cathodes [6]. Stockpiling large volumes of spent LIBs may lead to significant dangers, such as burning or blasting, which can be triggered by a single unit cell [6]. Moreover, as mentioned above, reused LIBs should ideally be recycled to regenerate valuable transition metals. The common recycling methods are based on pyrometallurgy [7], hydrometallurgy [4,8], biometallurgy [7], mechanical process [9,10], or their combination [11–13]. However, most of these recycling methods have several disadvantages when applied to LIBs, which hampers their large-scale application. The need for special anti-chemical-corrosion equipment and the use of high temperatures (1400°C or higher) increase the cost for regeneration of metals from spent LIB cathodes. Harmful exhaust fumes and strong caustic reagents, such as nitric and sulfuric acids, can easily lead to corrosion and pose a danger to workers and the environment. Moreover, the simultaneous dissolution and extraction of all kinds of metals from recycled LIB cathodes are difficult because of their different solubilities. Therefore, a sustainable recycling strategy for regenerating cathodes from spent LIBs must be

[1] State Key Laboratory of Marine Resource Utilization in South China Sea, School of Materials Science and Engineering, Hainan University, Haikou 570228, China
[2] Department of Materials Science and Engineering, and Center for Functional Photonics (CFP), City University of Hong Kong, Hong Kong S.A.R. 999077, China
[3] School of Materials Science and Engineering, Key Laboratory of Advanced Ceramics and Machining Technology of Ministry of Education, Tianjin University, Tianjin 300072, China
[4] Jiangsu Genox Environmental Engineering Technology Co., Ltd., Nanjing 210012, China
* Corresponding author (email: yida.deng@tju.edu.cn)

developed. Several new concepts and methods have emerged recently, but they are still on the laboratory scale. Moreover, the expansion of the use of spent LIBs into practical application, especially for their implementation in the loop of a circular economy, is difficult [14–17]. A practical, sustainable recycling strategy should be comprehensively evaluated from the perspectives of productivity, economic effectiveness, environmental friendliness, and safety.

In this study, we present an ultrafast carbothermal shock (CTS) treatment for the regeneration of cathodes of spent LIBs into multifunctional electrocatalysts. The end-of-life LIB with the most common commercial cathode $LiNi_{0.8}Mn_{0.1}Co_{0.1}O_2$ (NMC) was charged completely to maximize the delithiation degree. Then, this cathode was treated by the CTS process to convert NMC into the Ni/Ni-Co-Mn-O_x (N/NMCO) composite, which displayed an efficient multifunctional electrocatalytic performance toward oxygen evolution, oxygen reduction, and hydrogen evolution reactions (OER, ORR, and HER, respectively). As a result, an overall water-splitting device using N/NMCO as the cathode and anode showed a low overpotential of 1.61 V with a stable performance at different current densities. Moreover, N/NMCO can be used as electrodes in rechargeable aqueous Zn-air batteries (ZAB), which displayed a peak power density of 137 mW cm^{-2}, a specific capacity of 781 mA h g^{-1}, and outstanding stability within 35 h of continuous operation. Thus, our study paves the way toward sustainable regeneration of spent LIBs *via* a rapid, low-cost, and eco-friendly CTS strategy.

RESULTS AND DISCUSSION

High-temperature shock technology is a rapid and universal method to boost the crystallization of inorganic (nano)materials [18–20]. As a branch of this technology, CTS treatment applies carbon-based heat accumulators instead of metallic substrates. Thus, transition metal precursors can be reduced at high temperatures. We applied the CTS treatment for the regeneration of spent NMC cathodes of LIBs. As shown in Fig. 1a, b, and Fig. S1, the NMC was scraped from the spent LIB, loaded onto a carbon cloth substrate, and connected to the Cu electrodes of the power source. The carbon cloth was loaded onto the glass substrate and connected to the two sides of the heating equipment. Fig. 1b shows the heating process used for regenerating NMC cathodes. The heating temperature can be controlled by tuning the current density ($15 \geq I \geq 0$ A) and voltage ($30 \geq U \geq 0$ V). For the regeneration of NMC cathodes, the current density and voltage were set to 6 A and 15 V, respectively, and the temperature can reach 750°C. The temperature evolution during the CTS processing of NMC cathodes was recorded using an infrared thermometer. The heating and cooling rate reached 10^4–10^5 K s^{-1}, and the whole CTS process can be finished in 1–2 s (Fig. 1c). Such an ultrafast heating/cooling rate offers advantages for treating spent cathodes of LIBs, and the overall duration of CTS treatment is notably faster than other kinds of solid-state, chemical, and electrochemical processing.

The results provided in Fig. S2, along with the previously reported results, show that Ni in NMC contributes the largest proportion of specific capacity during the charge/discharge of LIBs [21–23]. Therefore, after long-term cycling and finally being deeply charged, most Li^+ ions in the LIB move toward the anode and thus generate a large number of metastable Ni^{3+}/Ni^{4+} in the spent NMC cathodes (Fig. 1d) [24–26]. The cations of transition metals Ni, Co, and Mn are in their high-valence states of Ni^{3+}/Ni^{4+}, Co^{3+}/Co^{4+}, and Mn^{4+}. As a result of the CTS treatment, part of the metastable Ni^{3+}/Ni^{4+} ions were reduced to zero-valent Ni nanoparticles, whereas several Ni^{3+}/Ni^{4+}, Co^{3+}/Co^{4+}, and Mn^{4+} cations were transformed into their respective oxides (Fig. 1e). This condition results in the formation of N/NMCO nanocomposites. In addition, the organic binder in the cathode, such as polyvinylidene fluoride, was transformed into graphitized carbon during the high-temperature CTS process, contributing to the high conductivity of the resulting composite. Thus the N/NMCO composite based on transition metals and their oxides would show promising electrocatalytic activities in OER and HER [27–29].

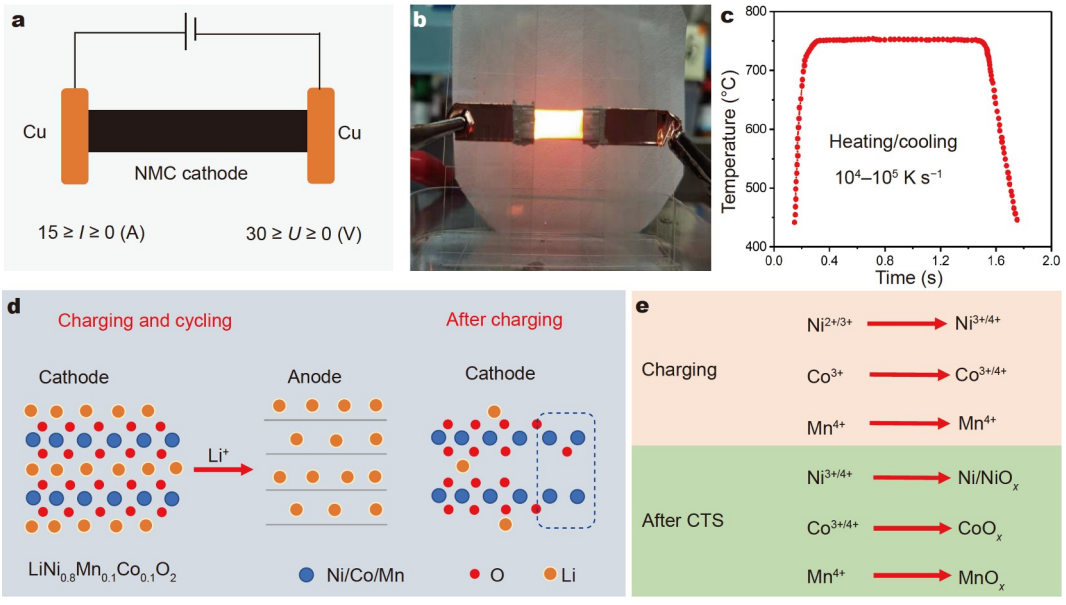

Figure 1 (a) Schematic illustration and (b) photograph of the CTS process applied to NMC cathode of LIBs. (c) Temperature evolution curve during the CTS. (d) Schematic illustration of the structural evolution and (e) expected conversion reactions of cathodes in LIBs after charging and CTS treatment.

The phase structure, morphology, and lattice structure of N/NMCO were analyzed and compared with those of the NMC after cycling (denoted as NMC-AC) and the pristine NMC that was never used. As observed in the X-ray diffraction (XRD) pattern (Fig. 2a), the crystal structure of N/NMCO shows different diffraction peaks from the NMC-AC and NMC, demonstrating that the spent cathode was transformed after the CTS process. Compared with the standard XRD patterns, the diffraction peaks of N/NMCO can be assigned to Ni (JCPDS 01-1260) and NMCO. In addition, NMCO is not a pure phase but a mixture of two or more transition metal oxides of NiO (JCPDS: 02-1216), MnO_2 (JCPDS: 44-0992), Ni_3CoO_4 (JCPDS: 03-0995), and Ni_6MnO_8 (JCPDS: 49-1295). Bimetallic oxides of Ni_3CoO_4 and Ni_6MnO_8 can be regarded as hetero-atom doping of Co and Mn into NiO or as composites of 3NiO-CoO and 6NiO-MnO_2, respectively, because the sizes of Ni, Co, and Mn atoms are quite similar, and NiO, CoO, and MnO_2 have similar crystal structures. Moreover, several diffraction peaks of NiO are at the same position as those of MnO_2 and Ni_6MnO_8. Therefore, the regenerated spent LIB cathodes contain Ni and NMCO, and no other impurities exist after the CTS process.

As presented in Figs S3 and S4, the morphology of NMC-AC is drastically different from that of the pristine NMC. Microspheres of pristine NMC (5–7 μm in diameter) were broken into submicron particles in NMC-AC, and the surface reconstruction occurred after the long-term cycling (Fig. S4b), which was consistent with the previous report [30]. After the CTS process, compared with that of NMC-AC, nanoparticles melted, and smaller grains agglomerated in N/NMCO (Fig. 2b, c). Ni, Co, and Mn were evenly distributed in the bulk of N/NMCO (Fig. S5). As shown in the transmission electron microscopy (TEM) image of N/NMCO (Fig. 2d), the primary nanoparticle sizes were in the range of 5–8 nm. The positions of the two adjacent NMCO and Ni nanoparticles were encircled by the blue and red lines, respectively, in Fig. 2e. Fig. 2f, g provide the high-resolution TEM (HRTEM) image and the selected area electron diffraction (SAED) pattern of the single NMCO nanoparticle within the blue area in Fig. 2e. The unevenly distributed lattice structure in Fig. 2f points out the co-existence of a mixture of several different transition metal oxides within this single NMCO particle. Fig. 2h, i provide the HRTEM image and the SAED pattern of the single Ni nanoparticle within the red area in Fig. 2e, respectively. All these data further confirm that spent NMC cathodes can be completely converted into a nanocomposite containing metallic Ni and several different transition metal oxides as a result of the CTS treatment.

X-ray photoelectron spectroscopy (XPS) was performed to evaluate the valence states of the transition metals in N/NMCO and NMC-AC. The survey of XPS spectra (Fig. S6) confirm the co-existence of Ni, Co, and Mn in N/NMCO, whose atomic ratio is very similar to that of NMC-AC (Table S1). Next, we quantitatively calculated the proportion of transition metals with different valence states in N/NMCO and NMC-AC based on the deconvolution of their high-resolution XPS spectra (Fig. 3a and Table S2). For the high-resolution Ni 2p spectra, the peaks of Ni $2p_{3/2}$ and Ni $2p_{1/2}$ are located at 856.3 and 873.4 eV, respectively. The signal of Ni^0 is at 853.7 eV. The peak position of Ni $2p_{3/2}$ in N/NMCO displays a negative shift compared with that in NMC-AC, demonstrating that the average valence state of Ni in N/NMCO is lower than that in NMC-AC. Moreover, the fitting results show that the proportion of Ni^{2+} increases in N/NMCO (Fig. 3b), demonstrating that several Ni^{3+} in NMC-

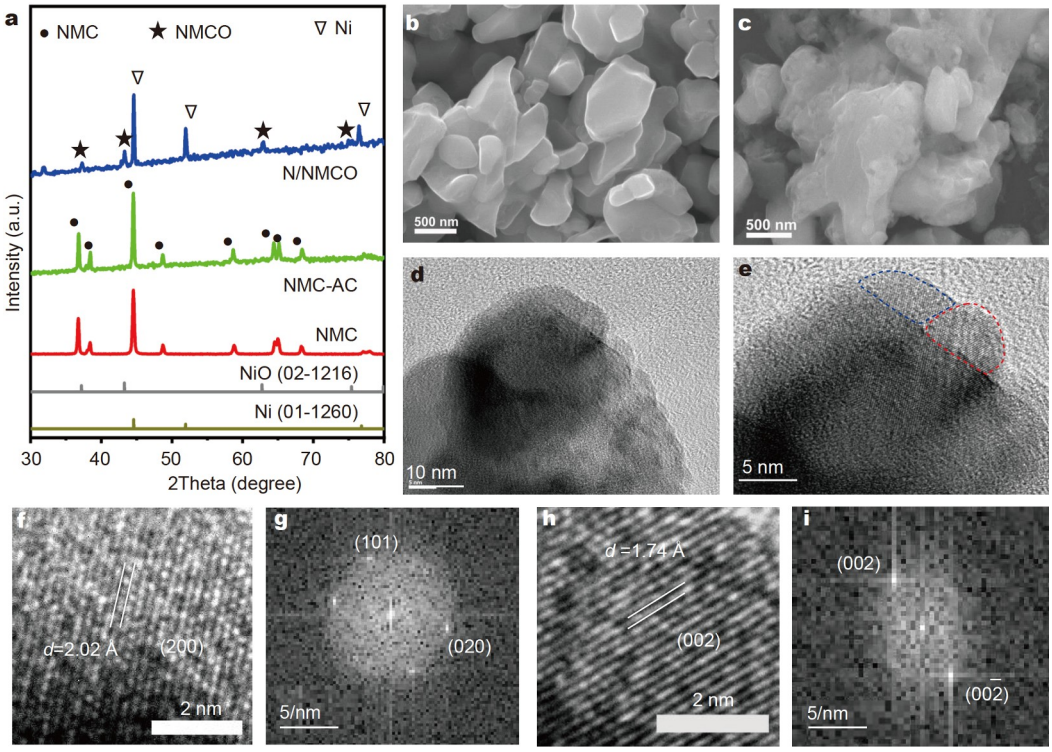

Figure 2 (a) XRD patterns of the pristine NMC, NMC-AC, and N/NMCO. Scanning electron microscopy (SEM) images of (b) NMC-AC and (c) N/NMCO. (d and e) TEM images of N/NMCO. The blue and red circles in (e) show the nanoparticles of NMCO and Ni, respectively; their corresponding HRTEM images and SAED patterns are shown in frames (f and g) and (h and i).

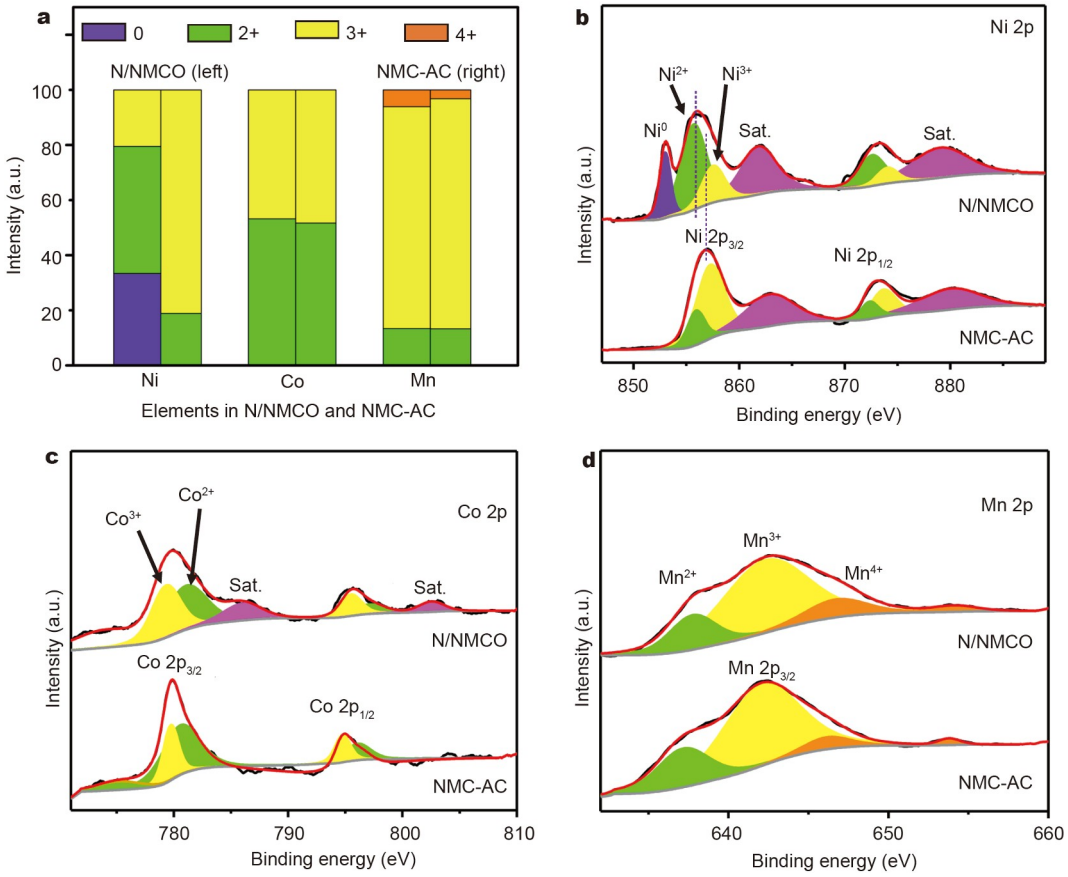

Figure 3 (a) The ratios of different valence states for Ni, Co and Mn in N/NMCO and NMC-AC. High-resolution XPS spectra of (b) Ni 2p, (c) Co 2p, and (d) Mn 2p in N/NMCO and NMC-AC.

AC were reduced to a lower valence state during the CTS treatment. The high-resolution Co 2p and Mn 2p spectra reveal that the Co $2p_{3/2}$, Co $2p_{1/2}$, and Mn $2p_{3/2}$ are located at 780, 795, and 642.4 eV, respectively. The XPS spectra of Mn 2p and Co 2p show no substantial change (Fig. 3c, d), indicating that their valence states remained the same in N/NMCO and NMC-AC. After long-term cycling and finally being deeply charged, Li^+ ions were extracted from the NMC cathode (Fig. 1d), thus causing several Ni ions to become metastable, which allows them to be easily reduced under CTS treatment. Thus, XPS data further confirm the co-existence of metallic Ni and transition metal oxides in the N/NMCO composite.

Electrocatalytic activity of N/NMCO in alkaline electrolyte was systematically analyzed using a standard three-electrode system and compared with that of the NMC-AC and two commonly used noble metal electrocatalysts, namely, Ir/C for OER and Pt/C for HER and ORR (Fig. 4). As observed from the linear sweep voltammetry (LSV) curves presented in Fig. 4a and the related data in Table S3, the overpotential (at 10 mA cm^{-2}) and the corresponding Tafel slope of N/NMCO are 285 mV and 47 mV dec^{-1}, respectively, which are superior to those of Ir/C (317 mV and 65 mV dec^{-1}) and NMC-AC (411 mV and 198 mV dec^{-1}). The difference in overpotentials become advantageous at a high current density of 50 mA cm^{-2} (Fig. 4c). Remarkably, the current density of N/NMCO (67 mA cm^{-2}) at 400 mV was about 2.7 and 13.2 times higher than those of Ir/C and NMC-AC, respectively (Fig. 4a). Such a superior current density demonstrates the outstanding OER catalytic activity of the N/NMCO composite, which is comparable to that of several other electrocatalysts, such as $NiSe_2/CoSe_2$, NiS_x, and $CoIn_2Se_4$ [31–33]. To evaluate the electrochemical active surface area of the electrodes, we studied double-layer capacitances (C_{dl}) by testing the cyclic voltammetry (CV) curves at different scan rates. As shown in Fig. 4d and Fig. S7, the C_{dl} value of N/NMCO (106.3 mF cm^{-2}) is 11.4 times higher than that of NMC-AC (9.3 mF cm^{-2}), which suggests that more catalytic active sites can participate in the OER process in this composite, thus resulting in its higher OER catalytic performance compared with Ir/C and NMC-AC. The long-term OER stability of N/NMCO can be observed from the great similarity of its LSV curves recorded before and after 1000 CV cycles (Fig. 4e) and the stable chronopotentiometry response presented in the inset of Fig. 4e. The Nyquist plots for OER (Fig. S8) were obtained by testing the electrochemical impedance spectroscopy (EIS) at 1.42 V (*vs.* reversible hydrogen electrode (RHE)), which also proved the faster ion and charge transfer rate and higher catalytic kinetics of N/NMCO compared with those of NMC-AC.

The development of bifunctional or multifunctional electrodes in which two or more reactions can occur on one electrode or on both the cathode and anode during cycling is an important contemporary task. Thus, we investigated the HER and ORR performance of N/NMCO. From the HER LSV curves provided in Fig. 4f, N/NMCO exhibits an overpotential of 112 mV at 10 mA cm^{-2}, which is 37 mV higher than that of commercial Pt/C (75 mV) but considerably lower than that of NMC-AC (482 mV), suggesting the promise of N/NMCO for hydrogen

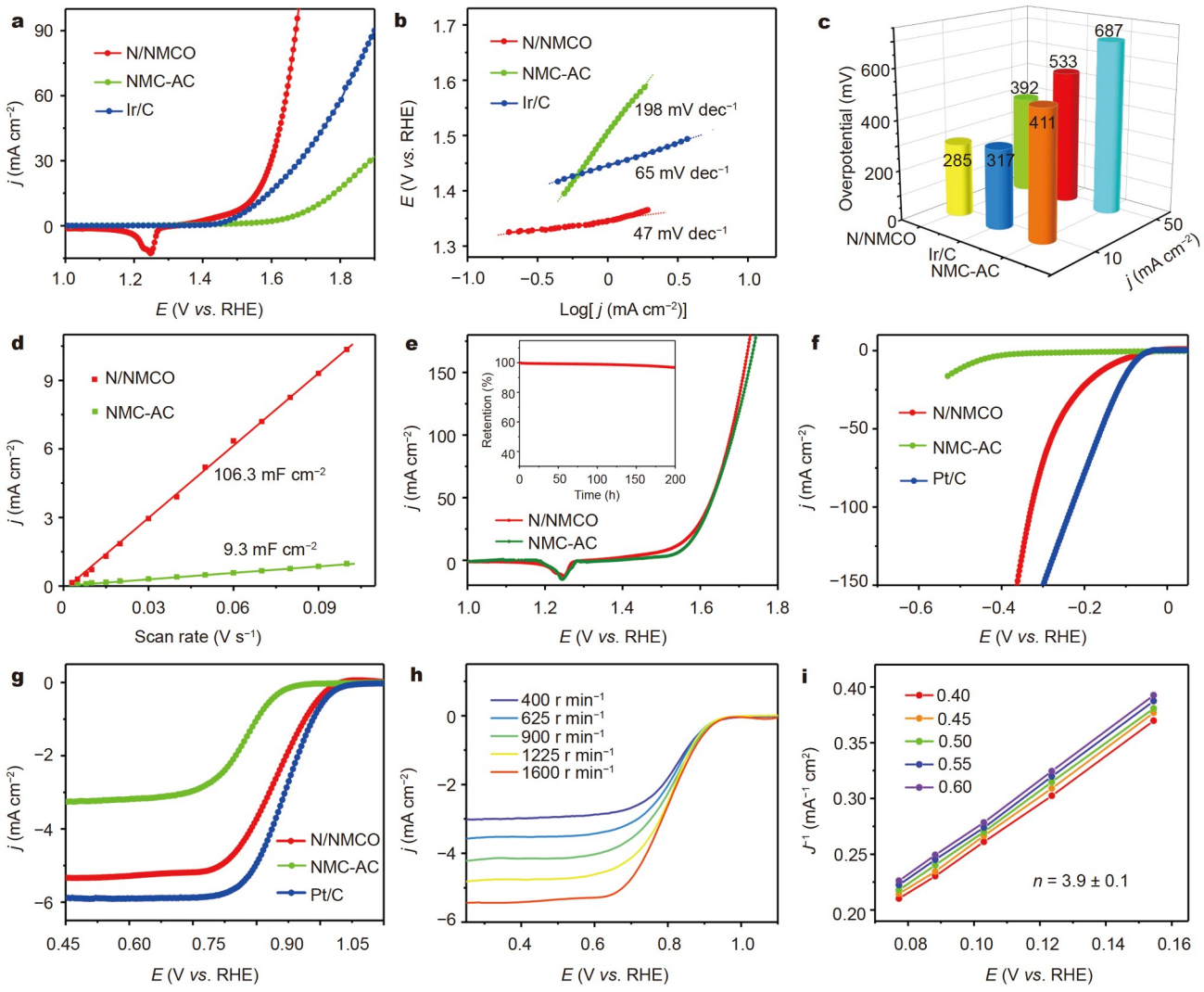

Figure 4 (a) OER LSV curves of the N/NMCO, NMC-AC, and Ir/C electrocatalysts tested in N_2 saturated 1.0 mol L^{-1} KOH solution at 5 mV s^{-1}; (b) the corresponding Tafel plots and (c) OER overpotentials of the three mentioned electrocatalysts at current densities of 10 and 50 mA cm^{-2}. (d) C_{dl} values of N/NMCO and NMC-AC. (e) OER polarization curves of N/NMCO before and after 1000 CV cycles; inset shows the chronopotentiometry response. (f) HER and (g) ORR LSV curves of the N/NMCO, NMC-AC, and Pt/C electrocatalysts. (h) ORR polarization curves of N/NMCO at different rotating speeds, and (i) the fitted Koutechy-Levich (K-L) plots at 0.4–0.6 V.

generation. The as-calculated HER Tafel (Fig. S9a) and Nyquist plots (Fig. S9b) tested at −0.065 V (*vs.* RHE) confirm the superior catalytic kinetics of N/NMCO compared with that of NMC-AC. Moreover, the N/NMCO displays remarkable HER catalytic stability with negligible degradation after more than 70 h (Fig. S10).

A rotating-ring disk electrode was used to assess the ORR activity. The ORR LSV curves shown in Fig. 4g suggest that N/NMCO displays an efficient oxygen reduction catalytic activity with the onset and half-wave potentials of 0.92 and 0.81 V, which are 0.02 and 0.04 V smaller than those of Pt/C. The superior ORR catalytic performance is also supported by the electron transfer number (*n*, Fig. 4i, calculated using Equation (S1) in Supplementary information). The polarization curves of N/NMCO at different rotation rates and the fitted K-L plots (Fig. 4h, i) obtained by Equation (S2) in Supplementary information reveal that N/NMCO catalyzes the ORR process *via* the quasi-4e$^-$ pathway, which is recognized as an efficient ORR pathway [15–18]. Such multifunctional catalytic activity of the N/NMCO composite can be attributed to the following factors: (i) simultaneous presence of Ni metal and NMCO oxides ensures its high conductivity and catalytic activity; (ii) small particle size and the increased electrochemically active surface area of N/NMCO ensure the exposure of favorable catalytic sites, accelerating the mass transfer kinetics.

Benefiting from the remarkable OER, HER, and ORR properties, the N/NMCO composites can serve as efficient and durable electrodes for overall water-splitting and rechargeable metal-air battery applications. Making use of the small potential difference (ΔV) between OER and HER calculated from OER and HER polarization curves (Fig. S11), which is very similar for N/NMCO electrodes (1.63 eV) and the {Pt/C + Ir/C} reference benchmark (1.62 eV), we assembled two overall water-splitting set-ups from either N/NMCO as the anode and cathode in 1.0 mol L^{-1} KOH (Fig. 5a) or mixed {Pt/C + Ir/C} electrodes in the same electrolyte. The LSV curves shown in Fig. 5b demonstrate that the water-splitting set-up with N/NMCO as dual electrodes required a voltage of 1.62 V to achieve 10 mA cm^{-2},

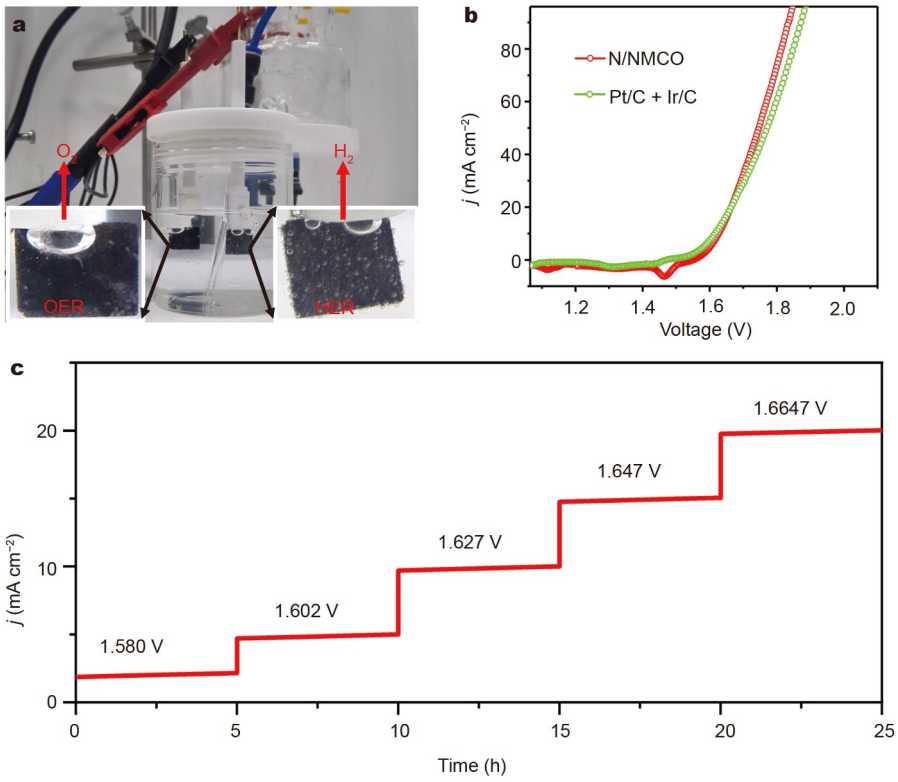

Figure 5 (a) Photograph of the overall water-splitting set-up with N/NMCO as the cathode and anode. (b) LSV curves of the overall water-splitting set-ups with either N/NMCO or mixed {Pt/C + Ir/C} electrodes. (c) Stability test of the overall water-splitting set-up using N/NMCO as cathode and anode with different current densities for several steps, with each step lasting for 5 h.

which is very comparable to the case of the mixed noble metal electrodes (1.61 V). The Faradaic efficiency of N/NMCO for water splitting was evaluated by comparing the gas amount between experimental and theoretical results (Fig. S12). The results show that the molar ratio of H_2:O_2 is nearly 2:1, and the experimental findings are consistent with theoretical values, suggesting a Faradaic efficiency of nearly 100%. The durability of the N/NMCO-based water splitting set-up was evaluated at different current density steps ranging from 2 to 20 mA cm^{-2} (Fig. 5c). The overpotential and current density are stable for at least 5 h during each step, indicating the outstanding stability for practical water splitting.

Furthermore, aqueous rechargeable ZABs were assembled by employing either N/NMCO composite or the mixed noble electrocatalysts {Pt/C + Ir/C} as the cathode, zinc plate as the anode, and a mixture of $ZnCl_2$ (0.2 mol L^{-1}) and KOH (6.0 mol L^{-1}) solutions in water as the electrolyte (Fig. 6a). The N/NMCO-based ZAB displays an open-circuit potential of 1.35 V, which remains stable for at least 20 h (Fig. S13). The polarization curves shown in Fig. 6b suggest that the N/NMCO-based ZAB offers better charge/discharge performance than the mixed noble metal-based ZAB. The peak power density of N/NMCO reaches 137 mW cm^{-2}, which is ~30% higher than that of the ZAB based on {Pt/C + Ir/C} cathode (Fig. 6c). Moreover, the specific capacity of N/NMCO cathode through galvanostatic discharging at 10 mA cm^{-2} reaches 781 mA h g^{-1} (Fig. 6d), which is higher than that for the {Pt/C + Ir/C} cathode (652 mA h g^{-1} at 10 mA cm^{-2}). The cycling profile of the N/NMCO-based ZAB (Fig. 6e) shows a charging potential of 1.96 V and discharging potential of 1.25 V, implying that the voltage gap is 0.71 V, and the round-trip efficiency is as high as 63%. These results are consistent with the trend of potential differences between OER and ORR of the N/NMCO, and the {Pt/C + Ir/C} benchmark as shown in Fig. S14, which were calculated from OER and ORR polarization curves. In addition, the cycling stability of N/NMCO is better than that of the mixed noble metal electrocatalysts (Fig. 6e).

In this work, we developed the CTS treatment strategy for regenerating spent cathodes of LIB into multifunctional electrodes for catalyzing HER, OER, and ORR. The as-assembled water splitting and ZAB devices provide promising applications of the regenerated catalysts for clean-energy conversion and storage. Here, we provide several viewpoints to further improve the utilization efficiency of waste cathodes. First, optimizing the microstructure of regenerated catalysts possesses great potential for further improving their catalytic efficiency and durability. In our following work, we will pay more attention to increasing the specific surface area, introducing atomic defects, etc., with the aim of enlarging the active site exposure. Second, the intrinsic activity of metallic sites needs to be optimized further. The local bonding environment and electronic structure of the regenerated catalysts should be well tuned by introducing heteroatoms, constructing interfaces, etc. Finally, the practical large-scale application of the regenerated catalysts needs to be explored. The final goal of regenerating spent cathodes is to put forward their practical application in real working conditions. Thus, the electrochemical performance of catalysts should be systematically investigated under practical conditions to enhance their efficiency and stability. In general, this work provides a new way for exploring the regeneration of spent cathodes of LIBs. The

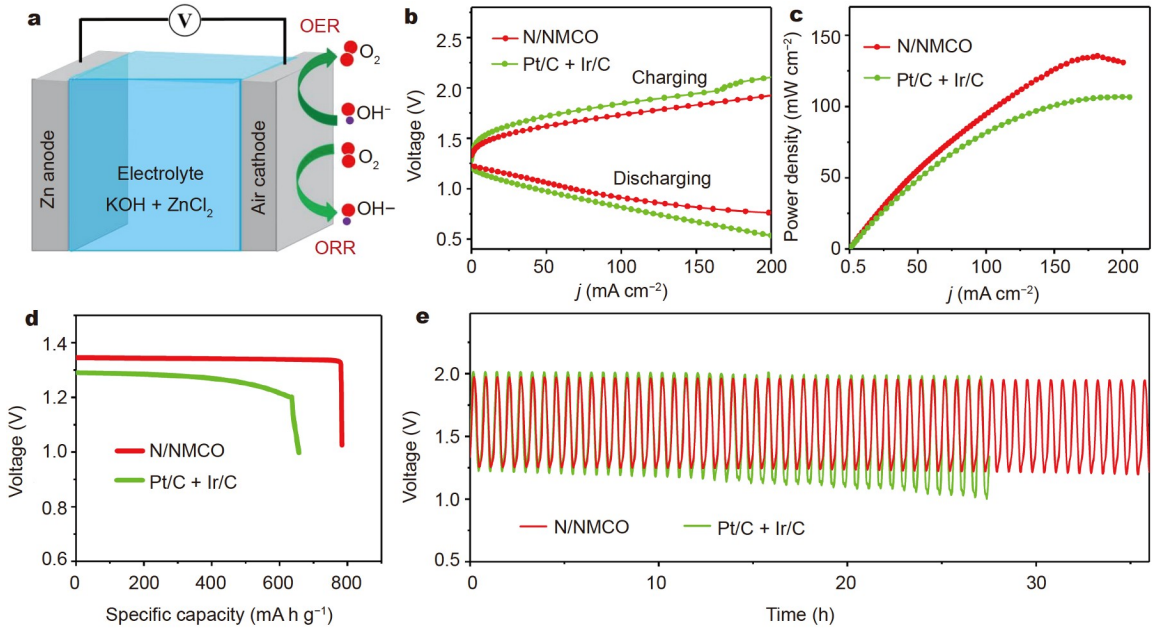

Figure 6 (a) Schematics of an aqueous ZAB. (b) Charge and discharge curves, (c) calculated power density, (d) specific capacity, and (e) cycling performance of the ZAB utilizing N/NMCO as the cathode (red curves) and comparision with the ZAB using {Pt/C + Ir/C} as the cathode (green curves).

further exploration and widespread application of large-scale regeneration of spent cathodes would be carried out in our future works.

CONCLUSIONS

With the ever-increasing demand for LIBs, efficient recycling methods are bound to appear to address spent LIB cathodes, to prevent environmental pollution, and to ensure the supply chain of strategic transition metals, such as Ni and Co. In this study, we introduced a regeneration process for spent LIB cathodes by CTS treatment. This process has the advantages of being eco-friendly, low cost, time-saving, and easy to apply for large-scale applications. The most common commercial spent cathode NMC was converted into N/NMCO as composite, which displayed multifunctional electrocatalytic activities for OER, ORR, and HER. As a result, the N/NMCO as composite showed advantageous electrochemical performance when applied as electrodes for the overall water splitting and in aqueous rechargeable ZABs. Our study paves the way for "converting waste into treasure" by regenerating spent cathodes of LIB into efficient electrodes, which can be applied for other clean-energy technologies. The same CTS treatment can be further optimized for recycling spinel, olivine, and disordered rock salt structures and thus becomes a widespread approach for developing closed-loop systems toward the large-scale application and sustainable regeneration of LIBs [34].

Received 20 December 2021; accepted 3 February 2022; published online 7 April 2022

1 Xiao J, Li J, Xu Z. Recycling metals from lithium ion battery by mechanical separation and vacuum metallurgy. J Hazard Mater, 2017, 338: 124–131
2 Fan E, Li L, Wang Z, *et al.* Sustainable recycling technology for Li-ion batteries and beyond: Challenges and future prospects. Chem Rev, 2020, 120: 7020–7063
3 Tran MK, Rodrigues MTF, Kato K, *et al.* Deep eutectic solvents for cathode recycling of Li-ion batteries. Nat Energy, 2019, 4: 339–345
4 Chen X, Chen Y, Zhou T, *et al.* Hydrometallurgical recovery of metal values from sulfuric acid leaching liquor of spent lithium-ion batteries. Waste Manage, 2015, 38: 349–356
5 He LP, Sun SY, Song XF, *et al.* Leaching process for recovering valuable metals from the $LiNi_{1/3}Co_{1/3}Mn_{1/3}O_2$ cathode of lithium-ion batteries. Waste Manage, 2017, 64: 171–181
6 Harper G, Sommerville R, Kendrick E, *et al.* Recycling lithium-ion batteries from electric vehicles. Nature, 2019, 575: 75–86
7 Zheng X, Zhu Z, Lin X, *et al.* A mini-review on metal recycling from spent lithium ion batteries. Engineering, 2018, 4: 361–370
8 Yang Y, Xu S, He Y. Lithium recycling and cathode material regeneration from acid leach liquor of spent lithium-ion battery *via* facile co-extraction and co-precipitation processes. Waste Manage, 2017, 64: 219–227
9 Li J, Wang G, Xu Z. Environmentally-friendly oxygen-free roasting/wet magnetic separation technology for *in situ* recycling cobalt, lithium carbonate and graphite from spent $LiCoO_2$/graphite lithium batteries. J Hazard Mater, 2016, 302: 97–104
10 Guo Y, Li Y, Lou X, *et al.* Improved extraction of cobalt and lithium by reductive acid from spent lithium-ion batteries *via* mechanical activation process. J Mater Sci, 2018, 53: 13790–13800
11 Huang B, Pan Z, Su X, *et al.* Recycling of lithium-ion batteries: Recent advances and perspectives. J Power Sources, 2018, 399: 274–286
12 Chen WS, Ho HJ. Recovery of valuable metals from lithium-ion batteries NMC cathode waste materials by hydrometallurgical methods. Metals, 2018, 8: 321
13 Sun C, Xu L, Chen X, *et al.* Sustainable recovery of valuable metals from spent lithium-ion batteries using DL-malic acid: Leaching and kinetics aspect. Waste Manag Res, 2018, 36: 113–120
14 Jin H, Zhou H, Ji P, *et al.* ZIF-8/$LiFePO_4$ derived Fe-N-P Co-doped carbon nanotube encapsulated Fe_2P nanoparticles for efficient oxygen reduction and Zn-air batteries. Nano Res, 2020, 13: 818–823
15 Piątek J, Afyon S, Budnyak TM, *et al.* Sustainable Li-ion batteries: Chemistry and recycling. Adv Energy Mater, 2021, 11: 2003456
16 Lu Q, Wu H, Zheng X, *et al.* Encapsulating cobalt nanoparticles in interconnected N-doped hollow carbon nanofibers with enriched Co–N–C moiety for enhanced oxygen electrocatalysis in Zn-air batteries. Adv Sci, 2021, 8: 2101438
17 Liu H, Cheng J, He W, *et al.* Interfacial electronic modulation of Ni_3S_2 nanosheet arrays decorated with Au nanoparticles boosts overall water

splitting. Appl Catal B-Environ, 2022, 304: 120935
18 Wang C, Ping W, Bai Q, *et al.* A general method to synthesize and sinter bulk ceramics in seconds. Science, 2020, 368: 521–526
19 Li T, Zhai Y, He S, *et al.* A radiative cooling structural material. Science, 2019, 364: 760–763
20 Yao Y, Huang Z, Xie P, *et al.* Carbothermal shock synthesis of high-entropy-alloy nanoparticles. Science, 2018, 359: 1489–1494
21 Tian C, Nordlund D, Xin HL, *et al.* Depth-dependent redox behavior of $LiNi_{0.6}Mn_{0.2}Co_{0.2}O_2$. J Electrochem Soc, 2018, 165: A696–A704
22 Liu Y, Harlow J, Dahn J. Microstructural observations of "single crystal" positive electrode materials before and after long term cycling by cross-section scanning electron microscopy. J Electrochem Soc, 2020, 167: 020512
23 Wood M, Li J, Ruther RE, *et al.* Chemical stability and long-term cell performance of low-cobalt, Ni-rich cathodes prepared by aqueous processing for high-energy Li-ion batteries. Energy Storage Mater, 2020, 24: 188–197
24 Jung R, Morasch R, Karayaylali P, *et al.* Effect of ambient storage on the degradation of Ni-rich positive electrode materials (NMC811) for Li-ion batteries. J Electrochem Soc, 2018, 165: A132–A141
25 Li J, Downie LE, Ma L, *et al.* Study of the failure mechanisms of $LiNi_{0.8}Mn_{0.1}Co_{0.1}O_2$ cathode material for lithium ion batteries. J Electrochem Soc, 2015, 162: A1401–A1408
26 Steiner JD, Mu L, Walsh J, *et al.* Accelerated evolution of surface chemistry determined by temperature and cycling history in nickel-rich layered cathode materials. ACS Appl Mater Interfaces, 2018, 10: 23842–23850
27 Zheng X, Zhang Y, Liu H, *et al. In situ* fabrication of heterostructure on nickel foam with tuned composition for enhancing water-splitting performance. Small, 2018, 14: 1803666
28 Liu P, Ran J, Xia B, *et al.* Bifunctional oxygen electrocatalyst of mesoporous Ni/NiO nanosheets for flexible rechargeable Zn-air batteries. Nano-Micro Lett, 2020, 12: 68
29 Zheng X, Cao Y, Han X, *et al.* Pt embedded Ni_3Se_2@NiOOH core-shell dendrite-like nanoarrays on nickel as bifunctional electrocatalysts for overall water splitting. Sci China Mater, 2019, 62: 1096–1104
30 Tian C, Lin F, Doeff MM. Electrochemical characteristics of layered transition metal oxide cathode materials for lithium ion batteries: Surface, bulk behavior, and thermal properties. Acc Chem Res, 2018, 51: 89–96
31 Zheng X, Han X, Cao Y, *et al.* Identifying dense $NiSe_2/CoSe_2$ heterointerfaces coupled with surface high-valence bimetallic sites for synergistically enhanced oxygen electrocatalysis. Adv Mater, 2020, 32: 2000607
32 Zheng X, Han X, Zhang Y, *et al.* Controllable synthesis of nickel sulfide nanocatalysts and their phase-dependent performance for overall water splitting. Nanoscale, 2019, 11: 5646–5654
33 Wang J, Zheng X, Cao Y, *et al.* Developing indium-based ternary spinel selenides for efficient solid flexible Zn-air batteries and water splitting. ACS Appl Mater Interfaces, 2020, 12: 8115–8123
34 Zheng X, Xu Z, Li S, *et al.* Reversible Mn/Cr dual redox in cation-disordered Li-excess cathode materials for stable lithium ion batteries. Acta Mater, 2021, 212: 116935

Acknowledgements This work was supported by the National Natural Science Foundation of China (52177220), Hong Kong Scholar Program (XJ2020001), and the State Key Laboratory of Electrical Insulation and Power Equipment of Xi'an University (EIPE21203). The authors are thankful to Dr. Jing Mao, Dr. Jingfeng Zhang, and Bamo-Tech Ltd. for their assistance in SEM, TEM, and battery characterization.

Author contributions Zheng X proposed and designed the project and wrote the draft. Zhao X and Lu J performed the experiments. Li J and Miao Z helped analyze and discuss the data. Xu W provided the resources. Deng Y and Rogach AL conceived the study. All authors contributed to the general discussion.

Conflict of interest The authors declare that they have no conflict of interest.

Supplementary information Experimental details and supporting data are available in the online version of the paper.

Xuerong Zheng works at the School of Materials Science and Engineering, Hainan University. He has specialized in the synthesis of transition metal oxides, sulfides and selenides with controllable morphologies, phase structures, and surface/interface properties for the application in energy storage and conversion systems. He mainly studies the local environmental and electrical structure variation and energy storage mechanism of transition metals using multiscale synchrotron and neutron scattering, spectroscopic, and imaging techniques, combining with the theoretical calculations.

Yida Deng was awarded "Changjiang Scholar" in 2021, and moved from Tianjin University to Hainan University as a chair professor. He has extensive experiences in the controllable synthesis of efficient electrocatalysts, such as noble and non-precious metallic nanomaterials, as well as their chalcogenides. His interest also includes the advanced energy storage and conversion systems, such as metal-air batteries and water splitting devices using the electrocatalysts as both cathodes and anodes.

超快碳热冲击将废旧锂电池正极材料变废为宝制备多功能电极用于水分解和可充锌空气电池

郑学荣[1,2,3], 赵鑫[2], 芦俊达[1], 李纪红[1], 苗政培[1], 许成[4], 邓意达[1,3*], 罗德礼[2]

摘要 随着锂离子电池在电动汽车和日常电子器件中的应用越来越广泛, 亟需开发废旧锂电池电极材料回收技术. 本文提出采用超快碳热冲击的方法将锂电池正极材料$LiNi_{0.8}Mn_{0.1}Co_{0.1}O_2$快速转化成Ni/Ni-Mn-Co-O (N/NMCO)复合材料, 其在氧析出(OER)、氧还原(ORR)、氢析出(HER)等反应中表现出优异性能. N/NMCO复合材料可以被同时用于电解水器件的正极和负极, 并用于锌空气电池的正极, 电池比容量可达781 mA h g^{-1}, 能量密度达到137 mW cm^{-2}, 充放电压差仅为0.71 V, 且可以稳定运行超过30 h. 本工作提供了一种"变废为宝"的策略, 将废旧锂离子电池正极材料转化为高效电极材料用于其他能源存储与转换器件中.

